

The BBGKY hierarchy for ultracold bosonic systems: II. Applications

Sven Krönke^{1,2,*} and Peter Schmelcher^{1,2,†}

¹*Zentrum für Optische Quantentechnologien, Universität Hamburg,
Luruper Chaussee 149, 22761 Hamburg, Germany*

²*The Hamburg Centre for Ultrafast Imaging, Universität Hamburg,
Luruper Chaussee 149, 22761 Hamburg, Germany*

(Dated: December 5, 2017)

In this work, which is based on our previously derived theoretical framework [1], we apply the truncated Born-Bogoliubov-Green-Kirkwood-Yvon (BBGKY) hierarchy for ultracold bosonic systems with a fixed number of particles to two out-of-equilibrium scenarios, namely tunneling in a double-well potential and an interaction quench in a harmonic trap. The efficient formulation of the theory provided in [1] allows for going to large truncation orders such that the impact of the truncation order on the accuracy of the results can be systematically explored. While the short-time dynamics is found to be excellently described with controllable accuracy, significant deviations occur on a longer time-scale for a sufficiently strong interaction quench or the tunneling scenario. These deviations are accompanied by exponential-like instabilities leading to unphysical results. The phenomenology of these instabilities is investigated in detail and we show that the minimal-invasive correction algorithm of the equation of motion as proposed in [1] can indeed stabilize the BBGKY hierarchy truncated at the second order.

I. INTRODUCTION

Understanding the impact of correlations on many-body quantum systems constitutes a major prerequisite for designing and controlling quantum matter. In these regards, ultracold atoms provide a highly flexible platform due to their isolatedness from an environment and their controllability, which allows for realizing a great variety of physical situations (variable trap geometries and interactions) and thereby for studying many-body effects in a systematic, unprecedented manner [2–4]. At the same time, this flexibility constitutes a challenge for theoretical approaches due to the wide range of particle numbers and interaction strengths involved.

While there has been tremendous progress in developing highly advanced wavefunction propagation method such as the time-dependent tensor-network approaches [5, 6] or the Multi-Configuration Time-Dependent Hartree method for Bosons (MCTDHB) [7], describing an ultracold gas of thousands or even hundred-thousands of atoms with the inherent correlations taken accurately into account is not within the immediate reach of methods aiming at the full many-body wavefunction. In such situations, an effective description of relevant subsystems of the complete many-body system appears to be much more appropriate. Here, we consider such a description of reduced density operators corresponding to few-particle subsystems of an ultracold bosonic quantum gas by means of the appropriately truncated Born-Bogoliubov-Green-Kirkwood-Yvon (BBGKY) hierarchy of equations of motion in its quantum version [8–12].

While there are numerous theoretical works on the BBGKY hierarchy and its truncation (see the references in [1] as well as e.g. [12] for an overview), the literature on the accuracy and stability of the truncated BBGKY equations of motion (EOM) in dependence on the truncation order by explicit numerical simulations is - to the best of our knowledge - limited [13–19]. Actually, most studies deal with fermions (for bosons, see [20–22] as well the BBGKY-related approaches [23–30]) and are based on the truncation of the BBGKY hierarchy after the second order.

For this reason, the purpose of this work is to comprehensively study the accuracy of BBGKY simulations of the non-equilibrium dynamics of finite ultracold bosonic ensembles when systematically increasing the truncation order in the framework of a cluster-expansion based closure approximation. While the immediately preceding work [1] covers the underlying theory and its efficient formulation, which allows for going to large truncation orders, we are here solely concerned with evaluating its accuracy and stability by numerical applications in two physically very transparent scenarios. The results for various truncation orders \bar{o} are compared to the MCTDHB simulations for the full N -particle wavefunction.

The first scenario is concerned with the tunneling dynamics of bosonic atoms in a double-well potential. Treating the system in the lowest-band tight-binding approximation allows us to go to large truncation orders without the need of dynamically optimizing the single-particle basis via the corresponding MCTDHB EOM [7]. Thereby, we probe solely effects stemming from the truncation of the BBGKY hierarchy. Here, we find the short-time dynamics to be excellently described by the BBGKY hierarchy and the accuracy to increase monotonously with increasing truncation order. For longer times, strong deviations are observed, which are linked to N -particle correlations becoming dominant as well as expo-

* skroenke@physnet.uni-hamburg.de

† pschmelc@physnet.uni-hamburg.de

nential instabilities of the truncated BBGKY EOM resulting in unphysical solutions. The phenomenology of these instabilities is analyzed in detail and we show that the minimal-invasive correction scheme for the BBGKY EOM (truncated at order $\bar{o} = 2$) [1] can stabilize these EOM indeed.

In the second scenario, we consider a harmonically trapped bosonic ensemble subjected to an interaction quench from the non-interacting regime to finite inter-particle repulsion. Here, we use the fully coupled system of the BBGKY EOM (6) of [1] and the MCTDHB EOM (5) of [1] for the time-dependent, variationally optimized single-particle basis. For low excitation energies, we find the system to be highly accurately described by the truncated BBGKY approach. For higher excitation energies, however, exponential instabilities again occur. Also in this case, we can stabilize the BBGKY EOM truncated at $\bar{o} = 2$ by our EOM correction scheme and obtain reasonably accurate results for longer times.

This work is organized as follows. While the main text is focused on the applications, namely the tunneling scenario in Section II and the interaction-quench scenario in Section III, technical comments on the numerical integration of the truncated BBGKY EOM are provided in Appendix A. Finally, we conclude in Section IV.

II. TUNNELING DYNAMICS IN A BOSE-HUBBARD DIMER

In this scenario, we assume that N bosonic atoms are loaded into an effectively one-dimensional double-well potential. Preparing the system in an initial state featuring a particle-number imbalance with a left and the right well allows for studying the tunneling dynamics of such a many-body system, which has been subject of numerous studies covering both mean-field [31, 32] and many-body calculations taking correlations into account [33–37]. Effects unraveled in such a realization of a bosonic Josephson junction cover macroscopic tunneling and self-trapping [31, 32, 38] as well a decay of tunneling oscillations due to the dephasing of populated many-body eigenstates of the post-quench Hamiltonian [33–37].

For sufficiently deep wells, the microscopic many-body Hamiltonian of this system can be well approximated by a two-site Bose-Hubbard Hamiltonian within the lowest-band tight-binding approximation

$$\hat{H} = -J(\hat{a}_L^\dagger \hat{a}_R + \hat{a}_R^\dagger \hat{a}_L) + \frac{U}{2}[\hat{n}_L(\hat{n}_L - 1) + \hat{n}_R(\hat{n}_R - 1)] \quad (1)$$

where $\hat{a}_{L/R}$ annihilates a boson in the lowest-band Wannier state localized in the left/right well and $\hat{n}_i \equiv \hat{a}_i^\dagger \hat{a}_i$ denotes the corresponding occupation-number operator of the site $i \in \{L, R\}$. The first term in (1) describes tunneling between the two wells weighted with the hopping amplitude $J > 0$. The second term refers to on-site

interaction of strength U and stems from the short-range van-der-Waals interaction between the atoms. For convenience, we take the hopping amplitude as our energy scale and state times in units of $1/J$.

The Bose-Hubbard dimer features an almost trivial computational complexity since the full many-body wavefunction depends only on $C_2^N = N + 1$ complex-valued coefficients such that the corresponding time-dependent Schrödinger equation can be numerically exactly solved for very large atom numbers. So there is no need for an alternative computational approach here. On the other hand, this system can serve as a good playground for analyzing the properties of the truncated BBGKY approach because (i) the corresponding numerically exact solution is available and (ii) we can easily represent RDMs of large order without using a dynamically optimized truncated single-particle basis. This allows for systematically investigating the accuracy of our results solely in dependence on the truncation order \bar{o} .

In the following, we consider the initial state $|\Psi_0\rangle = |N, 0\rangle$ with all atoms located in the left well and focus on the tunneling regime by setting the dimensionless interaction parameter $\Lambda = U(N - 1)/(2J)$ to 0.1, i.e. well below the critical value $\Lambda_{\text{crit}} = 2$ for self-trapping [31, 32]. In the weak interaction regime $\Lambda \ll 1$, beyond mean-field effects such as the aforementioned collapse of tunneling oscillation [33] and the universal formation of a two-fold fragmented condensate out of a single condensate [36] are expected to play a significant role after the time-scale $t_{\text{mf}} \approx \sqrt{2N + 1}/(J\Lambda)$, the so-called quantum break time [37].

Most of the following calculations deal with $N = 10$ atoms such that $t_{\text{mf}} \approx 46/J$. For comparison, we also increase N to 100 atoms while keeping Λ constant, which results in a longer quantum break time of $t_{\text{mf}} \approx 142/J$. We analyze the accuracy of the truncated BBGKY hierarchy approach in three steps. First, we inspect the particle-number imbalance, a highly-integrated quantity characterizing the tunneling dynamics, second turn to the eigenvalues of the lowest-order RDMs, which constitute a highly sensitive measure for correlations, and third compare the whole lowest order RDMs to the corresponding exact results. For a deeper interpretation of these findings, we finally analyze the exact results for the whole N -particle wavefunction as well as for the corresponding o -particle correlations. Finally, we investigate the performance of the correction strategies outlined in Section V B of [1].

A. Particle-number imbalance

In order to study the tunneling dynamics, the imbalance of the particle numbers between the left and right well, $[(\hat{n}_L) - (\hat{n}_R)]/N$, is depicted in Figure 1 for $N = 10$ atoms. Focusing first on the inset, which shows the numerically exact results, we see the expected collapse of tunneling oscillations due to a dephasing of the populated

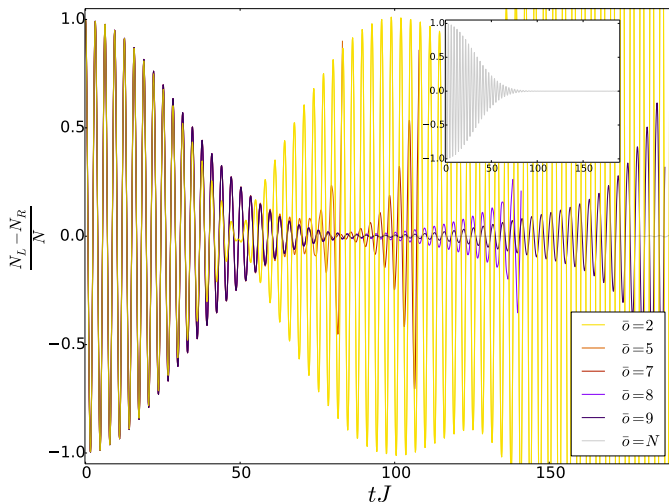


Figure 1. (color online) Time evolution of the particle-number imbalance $(N_L - N_R)/N$ with $N_i \equiv \langle \hat{n}_i \rangle$, $i \in \{L, R\}$ for various truncation orders \bar{o} . Inset: numerically exact solution of the many-body Schrödinger equation. Parameters: $N = 10$ atoms located initially in the left well, dimensionless interaction parameter $\Lambda = 0.1$.

post-quench Hamiltonian eigenstates. Indeed, this collapse happens on the time-scale $t_{\text{mf}} \approx 46/J$, while a corresponding Gross-Pitaevskii mean-field simulation would reveal undamped tunneling oscillations (not shown, see e.g. [37]). After $t \sim 200/J$, a revival of the tunneling oscillations emerges in the numerically exact calculation (not shown).

Turning now to the truncated BBGKY approach, we see that all truncation orders $\bar{o} \geq 2$ give good results for the first ~ 8 tunneling oscillations. Thereafter, the $\bar{o} = 2$ curves depart from both the exact and the higher truncation-order results, and features a premature maximal suppression of tunneling oscillations at $t \sim 50/J$. In the subsequent premature revival of tunneling oscillations unphysical values $|\langle \hat{n}_L \rangle - \langle \hat{n}_R \rangle|/N > 1$ are reached at about $t = 100/J$, indicating a lack of 1-RDM representability.

These findings suggest that higher-order correlations than \hat{c}_2 (see Section IV B 3 of [1] for the definition) play a significant role. Increasing the truncation order \bar{o} stepwise up to the maximally reasonable order $\bar{o} = N - 1 = 9$, we clearly see that the accuracy of our results improves systematically. The larger \bar{o} is, the more accurate is the collapse of the tunneling oscillations described. However, all non-trivial truncations $\bar{o} < N$ predict a premature revival of the tunneling oscillations, which goes hand in hand with a maximal suppression of the tunneling-oscillation amplitude to small but noticeable values (while the exact results do not feature noticeable oscillations at the corresponding times). We note that for $2 < \bar{o} < 10$ the simulations suffer from drastic instabilities of the EOM, being discussed in the subsequent Section, such that we had to stop them after a certain

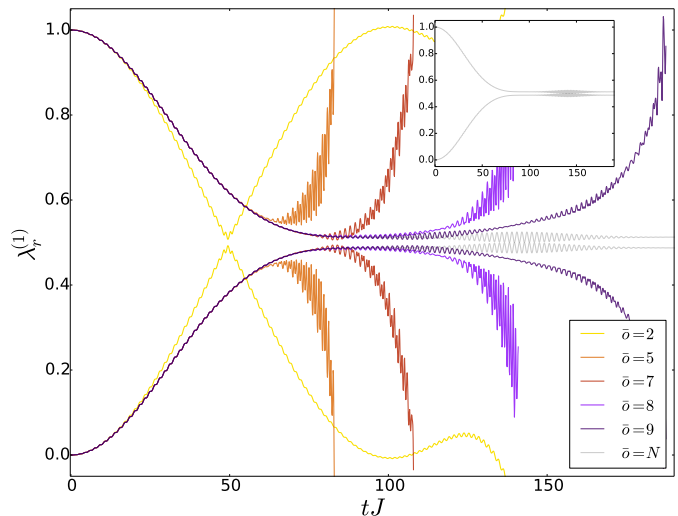


Figure 2. (color online) Natural populations of the 1-RDM for various truncation orders \bar{o} . Inset: numerically exact solution of the many-body Schrödinger equation. Parameters: same as in Figure 1.

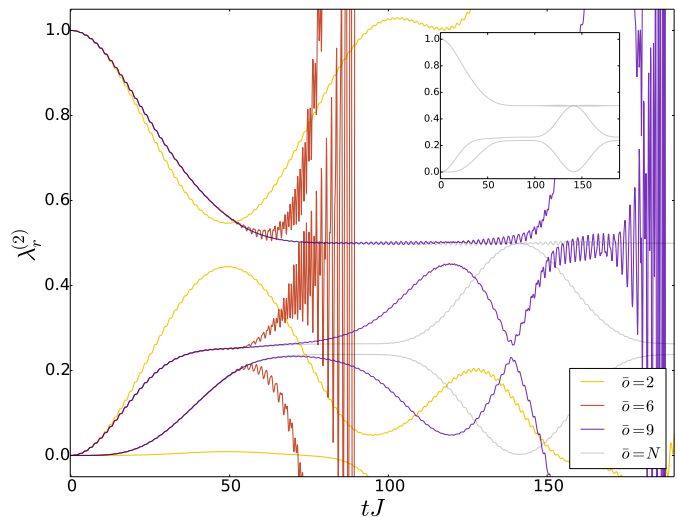


Figure 3. (color online) Natural populations of the 2-RDM for various truncation orders \bar{o} . Inset: numerically exact solution of the many-body Schrödinger equation. Parameters: same as in Figure 1.

time. This is why the corresponding curves in Figure 1 are not provided for the whole range of depicted times.

B. Natural populations

Next we analyze the eigenvalues $\lambda_i^{(o)}$ of the o -RDM, called natural populations¹ (NPs) in the following and start with the NPs of the 1-RDM NPs in Figure 2, which can diagnose beyond mean-field behavior. The numerically exact results (see corresponding inset) reveal dynamical quantum depletion leading to a two-fold fragmented condensate for $t \gtrsim 80/J$ with almost equal population of the corresponding NOs, $\lambda_1^{(1)} \approx 0.5 \approx \lambda_2^{(1)}$ (see also e.g. [36]). Strikingly fast oscillations in these NPs emerge and decay around $t \sim 140/J$, which we can connect to the periodical emergence and decay of a NOON state of the total system (see below).

The corresponding results of the truncated BBGKY approach feature a similar dependence on the truncation order \bar{o} as the particle-number imbalance does. While the $\bar{o} = 2$ prediction starts to deviate noticeably from the exact results already for $t \gtrsim 25/J$, we obtain trustworthy results for a longer time, the larger \bar{o} is chosen. In particular, the truncated BBGKY approach can accurately determine the achieved mean degree of fragmentation (see $\bar{o} = 8, 9$ results at $t \sim 100/J$). Even for the largest truncation order $\bar{o} = 9$, however, the truncated BBGKY simulations predict a premature and very fast revival of condensation (i.e. $\lambda_1^{(1)} \approx 1$), while this process starts only after $t \sim 200/J$ in the exact calculation and happens more slowly (not shown). Most importantly, this unphysical fast re-condensation overshoots the range of valid NPs such that the 1-RDM ceases to be positive semi-definite, indicating an exponential-like instability of the EOM.

While we have so far only studied the prediction of the truncated BBGKY approach for one-particle properties, we now inspect the NPs of the 2-RDM in Figure 3, also called natural geminal populations [40]. The exact dynamics (see the inset) features two important aspects, which we have also observed for the NPs of higher-order RDMs (not shown). (i) The dominant NP $\lambda_1^{(2)}$ first loses weight in favor for the other NPs. (ii) At about $t \sim 140/J$, all NPs are suppressed except for $\lambda_1^{(2)} \approx 0.5 \approx \lambda_2^{(2)}$. Having observed the latter feature for the NPs of all orders $o \in \{1, \dots, 9\}$, we may conclude that in this stage of the dynamics a subsystem of o particles occupies approximately only two o -particle states with almost equal probabilities. As we will see below, this finding is caused by the periodical emergence and decay of a NOON state of the total system which is discussed below.

Turning now to the predictions of the truncated BBGKY approach, we see again a systematic improvement of accuracy with increasing truncation order \bar{o} .

The maximal time for which the highest truncation order $\bar{o} = 9$ gives reliable results, however, has reduced from $t \sim 110/J$ for the 1-RDM NPs (see Figure 2) to $t \sim 70/J$ for the 2-RDM NPs (see Figure 3). Thereafter, the largest NP $\lambda_1^{(2)}$ is well described until $t \sim 130/J$, while the other two NPs already show strong deviations: it seems that the emergence of the feature (ii) discussed above happens premature, name at about $t \sim 120/J$. Furthermore, we also witness the exponential-like instabilities leading to 2-RDM NPs outside the interval $[0, 1]$.

In order to analyze how this unphysical behavior emerges, we depict the first time $t_{\text{neg}}(o)$ when the lowest o -RDM NP $\lambda_{o+1}^{(o)}$ is smaller than the threshold $\epsilon = -10^{-10}$ for various o and different truncation orders \bar{o} in Figure 4 a). For fixed truncation order \bar{o} , $t_{\text{neg}}(o)$ decreases with increasing order o . This means that the representability defect of $\hat{\rho}_o$ lacking positive semi-definiteness starts at the truncation order $o = \bar{o}$ and propagates then successively to lower orders due to coupling via the collision integral. For most orders o , we moreover find that $t_{\text{neg}}(o)$ increases with increasing truncation order \bar{o} , which fits to the above findings regarding enhanced accuracy for larger \bar{o} (exceptions occur at order $o = 1, 2$ in particular for $\bar{o} = 2$).

Increasing the number of atoms to $N = 100$ while keeping the dimensionless interaction parameter $\Lambda = 0.1$ constant, we again find a monotonous decrease of $t_{\text{neg}}(o)$ with increasing o for fixed truncation order \bar{o} (see Figure 4 b)). This confirms the above finding that the lack of positivity successively propagates from higher to lower orders. In contrast to the $N = 10$ case, we only find an enhancement of $t_{\text{neg}}(o)$ with increasing \bar{o} for orders $o \geq 6$. In particular, we see that the largest truncation order considered, $\bar{o} = 12$, features the smallest $t_{\text{neg}}(o = 2)$. It is quite possible that the an ‘‘enhancement’’ of non-linearity with increasing truncation order \bar{o} (note that the applied closure approximation, cf. Section IV B 3 of [1], is a polynomial of degree $(\bar{o} + 1)$ in $\hat{\rho}_1$ and of degree $\lfloor (\bar{o} + 1)/o \rfloor$ in the cluster \hat{c}_o) is the reason why the BBGKY EOM are more prone to these instabilities for larger \bar{o} .

Having compared so far only certain aspects of o -particle properties, we finally aim at comparing the prediction of the truncated BBGKY approach for the whole o -RDM to the exact results.

C. Reduced density operators

For this purpose, we take the trace distance $\mathcal{D}(\hat{\rho}_o^{\text{tr}}, \hat{\rho}_o^{\text{ex}}) \equiv \|\hat{\rho}_o^{\text{tr}} - \hat{\rho}_o^{\text{ex}}\|_1/2$ [41] as a measure for deviations between the truncated BBGKY prediction for the o -RDM denoted by $\hat{\rho}_o^{\text{tr}}$ and the numerically exact result $\hat{\rho}_o^{\text{ex}}$. Here, $\|\cdot\|_1$ refers to the trace-class norm (also called Schatten-1 norm) being defined as $\|\hat{A}\|_1 \equiv \text{tr}(\sqrt{\hat{A}^\dagger \hat{A}})$ for any trace-class operator \hat{A} . For hermitian operators \hat{A} , $\|\hat{A}\|_1$ equals the sum of absolute values of \hat{A} 's eigenvalues.

¹ The terms ‘natural population’ and ‘natural orbital’ have originally been introduced for the 1-RDM only [39] but are employed for all orders in this work.

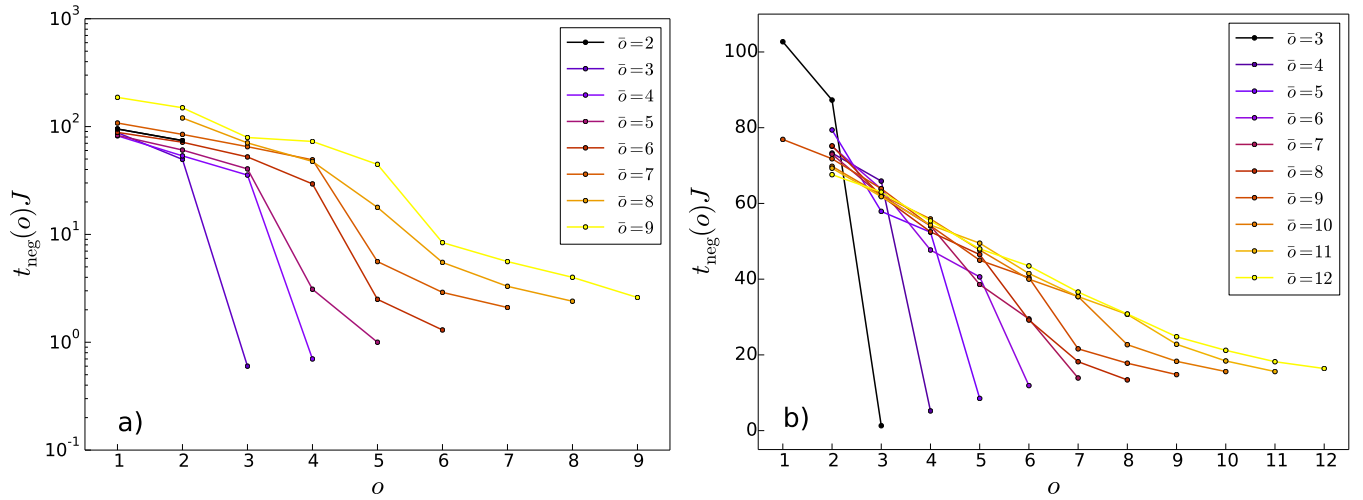


Figure 4. (color online) First time $t_{\text{neg}}(o)$ when the lowest o -RDM NP is smaller than $\epsilon = -10^{-10}$ in dependence on o for various truncation orders \bar{o} . a) Same parameters as in Figure 1. b) Same as a) but for the atom number N increased to 100 while keeping the interaction parameter $\Lambda = 0.1$ constant. The results for $\bar{o} = 2$ are not plotted in b) and read $t_{\text{neg}}(1) \approx 216/J$ as well as $t_{\text{neg}}(2) \approx 168/J$.

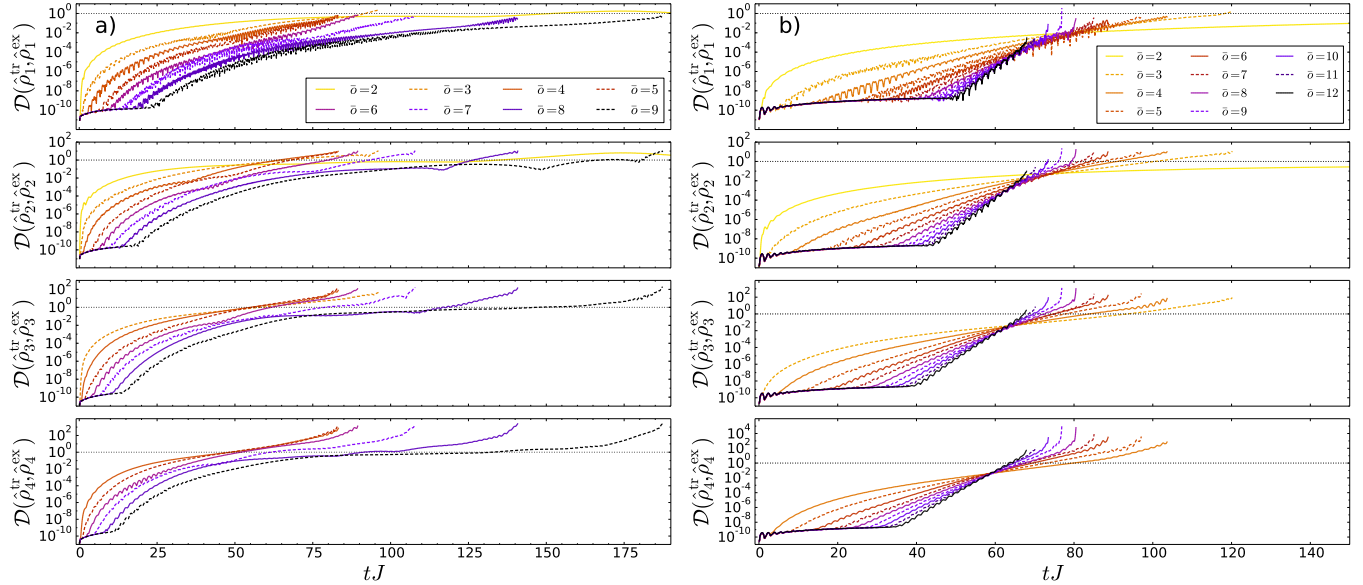


Figure 5. (color online) Time evolution of the trace distance $\mathcal{D}(\hat{\rho}_o^{\text{tr}}, \hat{\rho}_o^{\text{ex}})$ between the exact result and the truncated BBGKY prediction for the o -RDM ($o = 1, \dots, 4$) and various truncation orders \bar{o} . The dotted horizontal lines at unity ordinate value indicate the upper bound for the trace distance between two density operators (see main text). a) Same parameters as in Figure 1. b) Same as a) but for the atom number N increased to 100 while keeping the interaction parameter $\Lambda = 0.1$ constant.

By means of $\mathcal{D}(\hat{\rho}_o^{\text{tr}}, \hat{\rho}_o^{\text{ex}})$, one can estimate the maximal difference for the expectation values of any (trace-class) o -body observable \hat{A}_o as follows $|\text{tr}(\hat{A}_o \hat{\rho}_o^{\text{tr}}) - \text{tr}(\hat{A}_o \hat{\rho}_o^{\text{ex}})| \leq 2 \|\hat{A}_o\|_1 \mathcal{D}(\hat{\rho}_o^{\text{tr}}, \hat{\rho}_o^{\text{ex}})$, whose proof is reviewed in Appendix B. Moreover, given that its arguments are density operators (i.e. hermitian, positive semi-definite and trace one), the trace-distance is bounded by $\mathcal{D}(\hat{\rho}_o^{\text{tr}}, \hat{\rho}_o^{\text{ex}}) \in [0, 1]$ and can be interpreted as the probability that these two quantum states can be distinguished by the outcome of a single measurement [41].

In Figure 5, we depict $\mathcal{D}(\hat{\rho}_o^{\text{tr}}, \hat{\rho}_o^{\text{ex}})$ for the orders $o = 1, \dots, 4$ and various truncation orders \bar{o} , where subfigures a) and b) refer to the $N = 10$ and $N = 100$ case with the same interaction parameter $\Lambda = 0.1$, respectively. For fixed truncation order \bar{o} , we clearly see that the accuracy of the truncated BBGKY prediction for the o -RDM decreases with increasing order o . Up to a certain time, which depends on the order o , we moreover find $\mathcal{D}(\hat{\rho}_o^{\text{tr}}, \hat{\rho}_o^{\text{ex}})$ to decrease with increasing truncation order \bar{o} .

The instabilities of the truncated BBGKY EOM manifest themselves in the trace distance exceeding its upper bound $\mathcal{D}(\hat{\rho}_o^{\text{tr}}, \hat{\rho}_o^{\text{ex}}) \leq 1$ for density operators, implying that $\hat{\rho}_o^{\text{tr}}$ lacks to have trace one or to be positive semi-definite. Since the conservation of the initial RDM trace is ensured by the truncated BBGKY approach, violations of $\text{tr}(\hat{\rho}_o^{\text{tr}}) = 1$ can at most occur numerically if the system gets deep into the exponential-like instability (where we observe the truncated BBGKY EOM to become stiff such that the integrator has a hard time). Thus, exceeding the upper bound on the trace distance is connected to a lack of positive semi-definiteness and can be observed to happen earlier for increasing order o and fixed truncation order \bar{o} .

For the case of $N = 100$ atoms (see Figure 5 b)), we observe the additional particularity that in the vicinity of $t \sim 63/J$ the accuracy of the truncated BBGKY prediction for the o -RDM does not depend on the truncation order \bar{o} , which happens slightly earlier for larger o . Before this point, a systematic increase of accuracy is observed for increasing truncation order \bar{o} . Thereafter, lower truncation orders give (slightly) better results than higher ones. Furthermore, while in the $N = 10$ case one-body properties (such as e.g. the particle-number imbalance) can be described with reasonable accuracy up to $t \sim 2 t_{\text{mf}}$ (when the collapse of tunneling oscillations has already taken place), the instabilities hinders us to obtain accurate results for t larger than about $0.56 t_{\text{mf}}$ in the case of $N = 100$ (at this time, the tunneling oscillation amplitude is still significant).

D. Many-body state and o -particle correlations: exact results

In order to obtain physical insights in the above findings, we finally come back to the numerically exact results for $N = 10$ and measure the strength of o -particle correlations (see the definition given in Section IV B 3 of [1]) in terms of $\|\hat{c}_o\|_1$ in Figure 6 a). From the inset, we infer that the correlations initially build up in a hierarchical manner. First, only two-particle correlations start to play a role, then three-particle correlations and so on. This hierarchy in $\|\hat{c}_o\|_1$ holds, however, only until $t \sim 8/J$, when the ordering of the $\|\hat{c}_o\|_1$'s with respect to the order o starts to become reversed. After a certain point, N -particle correlations become the most dominant ones. This holds in particular in the vicinity of $t \sim 140/J$, where we have observed fast oscillations in the NPs $\lambda_{1/2}^{(1)}$ and found for all orders $o = 1, \dots, 9$ that the RDMs feature approximately only two finite NPs $\lambda_1^{(o)} \approx 0.5 \approx \lambda_2^{(o)}$. At this stage of the dynamics, all clusters \hat{c}_o of odd order o are strongly suppressed.

For connecting the above findings regarding o -particle correlations to the full many-body state, we depict in the Subfigures 6 b) and c) the probability $|\langle N - n, n | \Psi_t \rangle|^2$ of finding n atoms in the right and $(N - n)$ atoms in the left well. For the early dynamics, we witness how

the system becomes delocalized in the Fock space such that the tunneling oscillations become suppressed (Subfigure 6 b)). At later times, around $t \sim 140/J$, we, however, find the system to periodically oscillate between a NOON state $(|N, 0\rangle + e^{i\theta}|0, N\rangle)/\sqrt{2}$ (with some phase $\theta \in \mathbb{R}$) and some broad distribution being approximately symmetric with respect to its maximum at about $n = 5$ (Subfigure 6 c)). Due to this approximate symmetry of the distribution around $n = 5$, the particle-number imbalance approximately equals $[\langle \hat{n}_L \rangle - \langle \hat{n}_R \rangle]/N \approx 0.5$, i.e. tunneling oscillations are still suppressed. This approximate symmetry moreover leads to a doubling of the oscillation frequency compared to the initial tunneling-oscillation frequency, which is most probably linked to the fast oscillations in $\lambda_{1/2}^{(1)}$. Finally, one can analytically show that the n -RDM of the above mentioned NOON state reads $\hat{\rho}_n = (|n, 0\rangle\langle n, 0| + |0, n\rangle\langle 0, n|)/2$, meaning that the state of an n -particle subsystem is an incoherent statistical mixture with all particles residing in the left (right) well with probability 0.5. Thereby, we can directly connect the fact that the RDMs of all orders feature approximately only two finite NPs of approximately equal value to the underlying many-body state. Coming back to the findings for $\|\hat{c}_o\|_1$ of Figure 6 a), we may conclude that a NOON state leads to strong high-order correlations \hat{c}_o such that truncating the BBGKY hierarchy by means of the applied cluster expansion cannot be expected to give accurate results.

In summary, we have seen following. (i) While the truncated BBGKY approach gives highly accurate results for short times with controllable accuracy via the truncation order \bar{o} , the BBGKY approach shows deviations at longer times. (ii) Exponential-like instabilities, induced by the non-linear truncation approximation, propagate from high to low orders and lead to unphysical results at a certain point. (iii) o -particle correlations arise very fast in this tunneling scenario and soon cease to be in decreasing order with respect to o . (iv) The system evolves into a NOON state being dominated by N -particle correlations.

There appear to be at least two plausible causes why the BBGKY approach fails at a certain point: First, the number of terms in the cluster expansion (23) of [1] drastically increases with the order o , which implies that clusters should decay fast for a controllable approximation. For example, at the largest truncation order considered above, $\bar{o} = 12$, the truncation approximation $\hat{\rho}_{13}^{\text{app}}$ already involves 100 terms. Our findings (iii) and (iv), however, might indicate that this system is not suitable for a truncation based on the o -particle correlations defined in Section IV B 3 of [1]. Other truncation approximations might be more suitable.

Second, the exponential-like instabilities, being connected to a lack of representability, might be the main cause for the failure of the BBGKY EOM at longer times. This hypothesis is supported by the fast break-down of the BBGKY approach in the $N = 100$ case for the truncation order $\bar{o} = 12$. For this reason, we analyze next

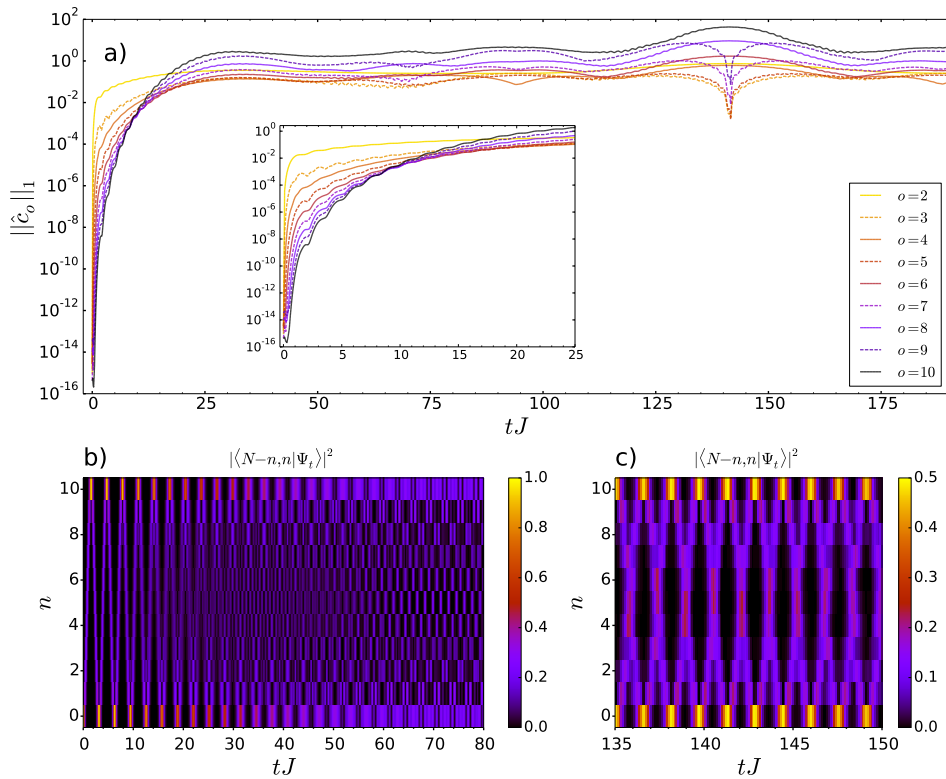


Figure 6. (color online) a) Time evolution of the cluster’s trace-class norm $\|\hat{c}_o\|_1$ for all orders o , obtained from the numerically exact solution of the time-dependent Schrödinger equation. Inset: zoom into early time dynamics. b) and c) Probability to find n atoms in the right and $(N - n)$ atoms in the left well, $|\langle N - n, n | \Psi_t \rangle|^2$, versus time for two characteristic stages of the dynamics. Parameters: same as in Figure 1.

the performance of the correction strategies outlined in Section V B of [1].

E. Performance of the correction algorithms

In the following, we first focus on the correction algorithms applied to the BBGKY hierarchy truncated at $\bar{o} = 2$. Thereafter, we comment on the performance of these algorithms if extended to larger truncation orders by means of a corresponding ansatz for the correction operator (see Section V B of [1]).

Figure 7 depicts the time evolution of the NPs $\lambda_i^{(2)}$ and the \hat{K}_2 eigenvalues ξ_i (see the definition given in Section V A of [1]) for the truncated BBGKY results without correction, with the iterative minimal invasive purification of the 2-RDM and the minimal invasive correction of the 2-RDM EOM in comparison to the exact results. Apparently, all cases deviate significantly from the exact results after $t \gtrsim 17/J$ so that we shall concentrate here solely on the stabilization performance of the correction algorithms.

Inspecting first the uncorrected results [Figures 7 (a.1),

(a.2)], we observe that the K -condition² (i.e. $\hat{K}_2 \geq 0$) diagnoses earlier a lack of representability compared to the D -condition (i.e. $\hat{\rho}_2 \geq 0$). For both operators, the falling of an eigenvalue below zero is accompanied by an avoided crossing which involves the next-larger eigenvalue (this is hardly visible in the case of the \hat{K}_2 eigenvalue where the avoided crossing happens at about $t \sim 71.5/J$). In fact, we have observed that level-repulsion “pushes” eigenvalues below zero in various other situations (see also Section III).

Now turning to the minimal invasive correction algorithms based on the 2-norm minimization of the correction operator \hat{C}_2 , we set the threshold ϵ below which an eigenvalue is regarded as negative to -10^{-10} . Let us first inspect the dimensionality of the optimization problem underlying both our purification algorithm of the 2-RDM and the correction algorithm of its EOM (see Appendix H of [1] for the details). The bosonic hermitian correction operator \hat{C}_2 can be parametrized by $m^2(m+1)^2/4 = 9$ real-valued parameters. Requiring \hat{C}_2 to be contraction-free and energy-conserving imposes

² We call this condition K - instead of G -condition, as commonly done, in order to stress that we operate with the original, more restrictive definition of the one-particle-one-hole RDM of [43].

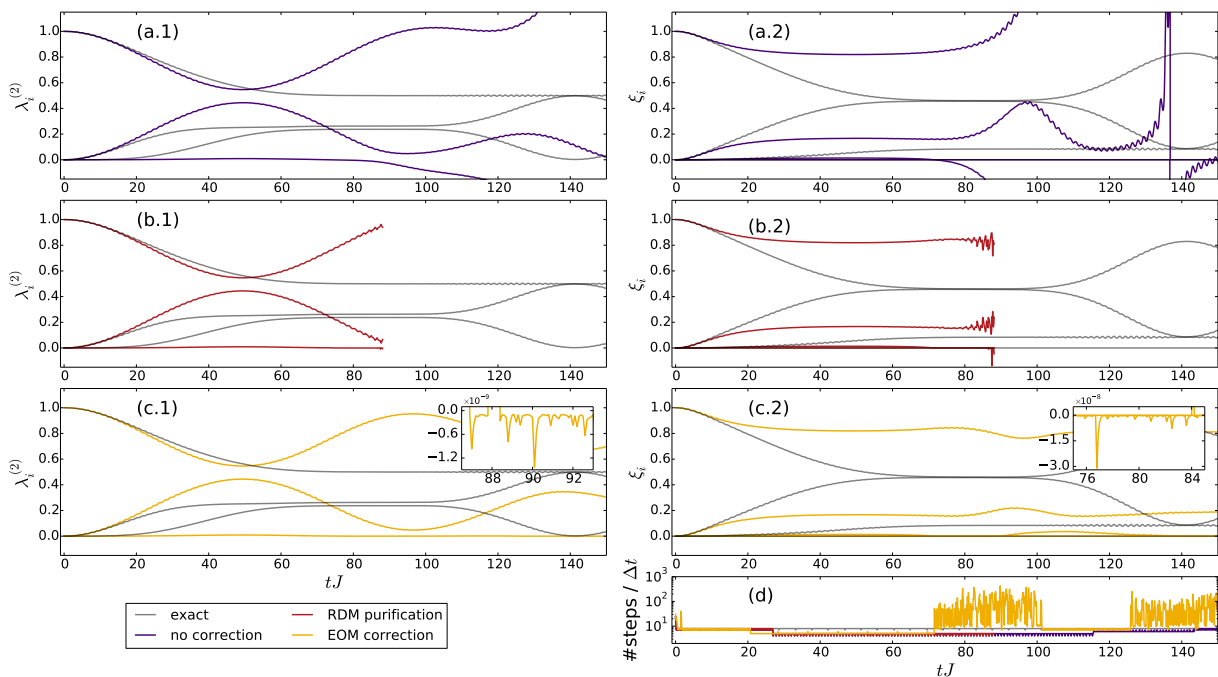


Figure 7. (color online) Comparison of the correction strategies outlined in Section V B of [1] (for the BBGKY hierarchy truncated at $\bar{o} = 2$). Left column: Time evolution of the NPs $\lambda_i^{(2)}$. Right column [except for (d)]: Time evolution of the \hat{K}_2 eigenvalues ξ_i . First row: Truncated BBGKY results without correction versus exact ones. Second row: Truncated BBGKY results with iterative minimal-invasive purification of the 2-RDM after each $\Delta t = 0.1/J$ (maximal number of iterations: 500). Third row: Truncated BBGKY results with minimal-invasive correction of the 2-RDM EOM (damping rate of negative eigenvalues: $\eta = 10J$). Insets of (c.1) and (c.2): close-ups showing the imposed exponential damping of negative eigenvalues. For both correction strategies, eigenvalues are regarded as negative if they are smaller than the threshold $\epsilon = -10^{-10}$. Subfigure (d): number of ZVODE integrator [42] steps per write-out time-step Δt . Parameters: same as in Figure 1.

$m^2 + 1 = 5$ constraints such that the system of linear equations corresponding to the constraints is underdetermined as long as the numbers of negative $\hat{\rho}_2$ eigenvalues d and negative \hat{K}_2 eigenvalues d' obey $d + d' < 4$.

Figure 7 (b.1) and (b.2) depict the results if the iterative minimal-invasive purification algorithm is applied after each $\Delta t = 0.1/J$. Clearly, we see that this correction algorithm induces strong noise in the \hat{K}_2 eigenvalues when the smallest eigenvalue ξ_i has reached significant negative values in the uncorrected BBGKY calculation [see subfigure (a.2)]. Actually, after $t = 86.5/J$, the iterative purification algorithm fails to converge after the maximal number of 500 steps. Thus, this iterative scheme fails to prevent that smallest eigenvalue is pushed to negative values due to level repulsion.

In a certain sense, we may view the iterative purification algorithm of the 2-RDM as being based on a fixed stepsize as well as perturbative. In each iteration step namely, we update $\hat{\rho}_2(t) \rightarrow \hat{\rho}_2(t) + \hat{\mathcal{C}}_2$ with $\hat{\mathcal{C}}_2$ shifting negative eigenvalues to zero in first-order perturbation theory. In the correction algorithm for the 2-RDM EOM, we effectively allow for variable update stepsizes by coupling the correction scheme to the integration of the EOM, i.e. to the employed integrator ZVODE [42] featuring adaptive stepsizes. Moreover, by imposing constraints on the

time-derivative of negative eigenvalues, we realize a non-perturbative correction scheme.

This can nicely be inferred from the insets of Figure 7 (c.1) and (c.2) showing a close-up of slightly negative eigenvalues. These are exponentially damped to zero, namely as e.g. $\xi_i(t + \tau) = \xi_i(t) \exp[-\eta\tau]$ for t and τ such that $\xi_i(t + \tau) < \epsilon$, with the chosen damping constant $\eta = 10J$. As a consequence, the truncated BBGKY EOM becomes stabilized and we have observed that the D - and K -representability condition are fulfilled to a good approximation for at least $t \leq 1000/J$ (times later than $t = 150/J$ not shown in Figure 7). When enforcing negative eigenvalues to be damped to zero, one might fear that eigenvalues accumulate in the range $[\epsilon, 0]$. This, however, is not the case as shown in the insets of Figure 7 (c.1) and (c.2) because no constraint on the time-derivative of an eigenvalue is enforced if its value exceeds the threshold ϵ such that the (corrected) EOM may lift this eigenvalue above zero. We finally remark that the number of integrator steps per Δt significantly increases in the vicinity of avoided crossings of $\hat{\rho}_2$ or \hat{K}_2 eigenvalues close to zero [see Figure 7 (d)]. This finding confirms the non-perturbative, adaptive nature of the EOM correction algorithm and at the same time highlights the significance of controlling such avoided crossings for a successful sta-

bilization of the truncated BBGKY EOM.

Without showing additional graphical illustrations, let us now briefly comment on the behavior of the correction algorithms for truncation orders $\bar{o} > 2$, using the Mazziotti ansatz [44] for the correction operators \hat{C}_o on orders $o > 2$ (see Section V B of [1]). Focusing first on the RDM purification, we have observed that $\hat{\rho}_{\bar{o}}$ can be kept positive semi-definite up to a few tens $1/J$ longer (compared to the uncorrected case) before this iterative correction algorithm fails to converge after 500 steps. Due to the losing of positive semi-definiteness in decreasing sequence with respect to the RDM order (see Figure 4), we found for $\bar{o} \geq 4$ that also $\hat{\rho}_{\bar{o}-1} \geq 0$ is valid for somewhat longer times compared to the uncorrected case. Unfortunately, however, this correction scheme fails to converge so early that it does not improve the timescale, on which the most important RDMs for making predictions for ultracold quantum gas experiments, namely $\hat{\rho}_1$ and $\hat{\rho}_2$, obey the considered representability conditions.

Extending the EOM correction scheme to higher truncation orders $\bar{o} > 2$ by means of the Mazziotti ansatz for the higher-order correction operators unfortunately proved to be quite unsuccessful. This failure manifests itself in an enormous increase of integrator steps per Δt , i.e. the EOM becoming stiff, in combination with the quadratic optimization problem for determining \hat{C}_2 having no solution, i.e. constraints contradicting one another. Unfortunately, we cannot tell whether the latter is a fundamental problem or whether it is only induced by the EOM to become stiff due to an inappropriate ansatz of \hat{C}_o for $o > 2$, potentially leading to integration errors.

To sum up, while we can successively stabilize the BBGKY EOM truncated at order $\bar{o} = 2$ by enforcing the D - and K -representability condition via a minimal invasive correction of the 2-RDM EOM, the issue of higher-order correlations becoming dominant after a certain time remains unsolved in this example. Since this tunneling scenario might well be unsuitable for a closure approximation based on neglecting certain few-particle correlations, we now turn to an example, where a BEC becomes only slightly depleted in the course of the quantum dynamics.

III. INTERACTION-QUENCH INDUCED BREATHING DYNAMICS OF HARMONICALLY TRAPPED BOSONS

In this application, we are concerned with collective excitations of N ultracold bosons confined to a quasi one-dimensional harmonic trap. In harmonic oscillator units (HO units), the corresponding Hamiltonian reads

$$\hat{H} = \sum_{i=1}^N \frac{\hat{p}_i^2 + \hat{x}_i^2}{2} + g \sum_{1 \leq i < j \leq N} \delta(\hat{x}_i - \hat{x}_j) \quad (2)$$

where we model the short-range van-der-Waals interaction by the contact potential [2] of strength g . Initially,

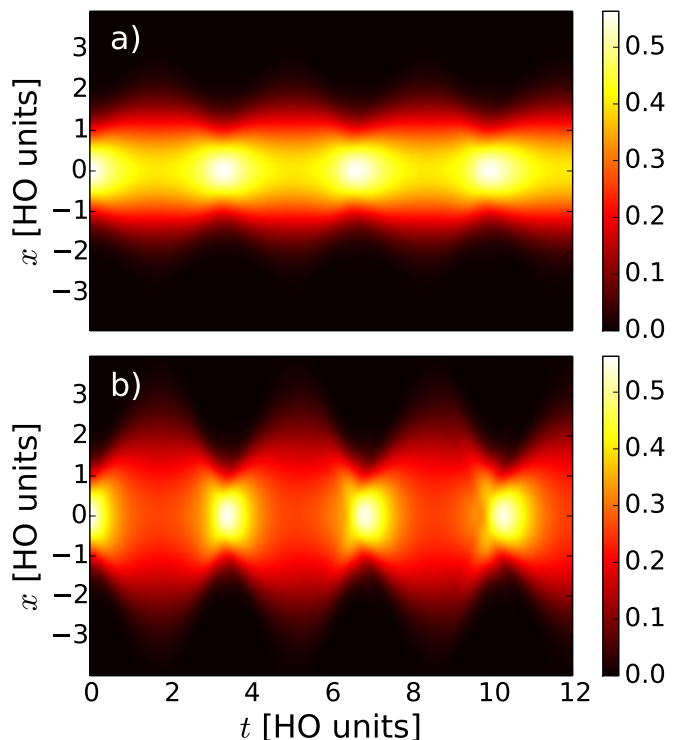


Figure 8. (color online) Time-evolution of the reduced one-body density $\rho_1(x; t) = \langle x | \hat{\rho}_1(t) | x \rangle$ for $N = 10$ [subfigure (a)] and $N = 30$ [subfigure (b)] bosons quenched from the non-interacting ground-state to a contact-interaction strength of $g = 0.2$. These results are obtained by MCTDHB simulations with $m = 4$ dynamically optimized SPFs.

we assume all atoms to reside in the ground state of the single-particle Hamiltonian, i.e. a Gaussian orbital, which is the exact many-body ground state in the absence of interactions. Then, the interaction strength is instantaneously quenched to $g = 0.2$ such that the ideal BEC becomes slightly depleted and its density performs breathing oscillations, i.e. expands and contracts periodically. This so-called breathing mode has been investigated theoretically as well as experimentally in different settings (see e.g. [45–51] for single-component systems and e.g. [52] for mixtures), and measuring its frequency proves to be useful for characterizing the interaction regime [53].

Before we discuss the results of the truncated BBGKY approach, let us first inspect the results of MCTDHB simulations with $m = 4$ dynamically optimized SPFs, which shall serve as the reference in the following. For representing the SPFs, a harmonic discrete variable representation [54, 55] with $n = 256$ ($n = 320$) grid points is employed for case of $N = 10$ ($N = 30$) particles. In Figure 8, we depict the time evolution of the reduced one-body density, i.e. the diagonal of the 1-RDM in position representation $\rho_1(x; t) = \langle x | \hat{\rho}_1(t) | x \rangle$, for $N = 10$ and $N = 30$ bosons. In both cases, we clearly see that the atomic density periodically expands and contracts. Since the interaction quench leads to a more than three

times larger interaction energy per particle of the ensemble of $N = 30$ atoms compared to $N = 10$ (at $t = 0$), the density of the former expands much further into the outer parts of the trap. In contrast to this, the density of the $N = 10$ atom ensemble seems to stay Gaussian (with a time-dependent width) to a good approximation, indicating that we operate in the linear-response regime here. We note that the quench leads to only a slight quantum depletion of at most 3% in both cases (see below).

In the following, we first show that the truncated BBGKY approach leads to stable results in the $N = 10$ case, whose accuracy can be systematically improved by increasing \bar{o} . Thereafter, we turn to the $N = 30$ case where we again encounter instabilities of the EOM and thus apply correction algorithms. We stress that for both cases we operate with $m = 4$ dynamically optimized SPFs, solving the truncated BBGKY EOM coupled to the MCTDHB EOM for the SPFs, which is in contrast to the Bose-Hubbard tunneling scenario of Section II.

A. Breathing dynamics of $N = 10$ bosons

In Figure 9, we show the time-evolution of the 2-RDM NPs for various truncation orders. Focusing first on the MCTDHB results, we see that correlations (in the sense of deviations from a Gross-Pitaevskii mean-field state where on all orders o there is only one finite NP $\lambda_1^{(o)} = 1$ and all other NPs vanish) repeatedly emerge and decay. The deviations from the NP distribution of a Gross-Pitaevskii mean-field state is approximately most pronounced when the density is most spread-out and become almost negligible when the density has approximately recovered its initial width [see Figure 8 a)].

While the truncated BBGKY results for $\bar{o} = 2$ feature significant deviations from the MCTDHB results, the results drastically improve when going to $\bar{o} = 3$ and become practically indistinguishable from the MCTDHB results already at the truncation order $\bar{o} = 4$. Actually, convergence of the 1-RDM NPs $\lambda_i^{(1)}$ is reached even at $\bar{o} = 3$ (not shown). Coming back to $\bar{o} = 2$, we point out that the 2-RDM quickly becomes indefinite where small negative eigenvalues are in particular pushed further to larger negative values when the density contracts to its initial width and small but positive NPs approach zero. As in the case of the above tunneling scenario, we interpret this finding as “induced” by level repulsion. Upon increasing the truncation order, we see that the 2-RDM stays positive semi-definite on the considered time-interval, which is a nice example for how increasing the accuracy of the closure approximation also stabilizes the truncated BBGKY EOM.

For a systematic comparison, we next compare the trace-class distance $\mathcal{D}(\hat{\rho}_o^{\text{tr}}, \hat{\rho}_o^{\text{ex}})$ between the truncated BBGKY result for the o -RDM, $\hat{\rho}_o^{\text{tr}}$, and the corresponding MCTDHB result, $\hat{\rho}_o^{\text{ex}}$, in Figure 10 a). We remark that although the SPFs of the truncated BBGKY approach obey the same EOM (5) of [1] as the dynamically

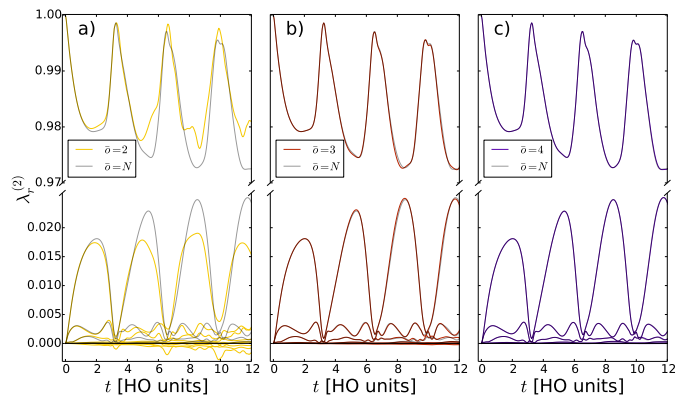


Figure 9. (color online) Natural populations of the 2-RDM for the truncation orders $\bar{o} = 2$ [a)], $\bar{o} = 3$ [b)] and $\bar{o} = 4$ [c)] in comparison to the MCTDHB results. Parameters: $N = 10$ atoms, post-quench interaction strength $g = 0.2$, $m = 4$ dynamically optimized SPFs.

optimized SPFs of the MCTDHB method, we cannot expect these two sets of SPFs to coincide because the 1- and 2-RDM entering the SPF EOM differ in general, which has to be taken into account when calculating $\mathcal{D}(\hat{\rho}_o^{\text{tr}}, \hat{\rho}_o^{\text{ex}})$. In stark contrast to the tunneling scenario, we see that the accuracy of the truncated BBGKY results for the 1- and 2-RDM systematically improves upon increasing \bar{o} for all considered times.

Finally, we quantify the strength of few-particle correlations in terms of $\|\hat{c}_o\|_1$, as extracted from the $\bar{o} = 7$ calculation [see Figure 10 a)]. Here, we see that the correlations stay bounded on the considered time interval and are ordered in a clear hierarchy, i.e. $\|\hat{c}_{o+1}\|_1(t) < \|\hat{c}_o\|_1(t)$. Apparently, these are ideal working conditions for the truncated BBGKY approach.

B. Breathing dynamics of $N = 30$ bosons

Next, let us increase the quench-induced excitation energy per particle by more than a factor of three when going to $N = 30$ bosons and keeping the post-quench interaction strength $g = 0.2$ the same. Similarly to the tunneling scenario, we first inspect the natural populations, then compare lowest order RDMs and finally evaluate the performance of the correction algorithms under discussion.

1. Natural populations

In Figure 11, we show the NPs of the 1- and 2-RDM for various truncation orders \bar{o} in comparison to the MCTDHB results. Similarly to the $N = 10$ case, we see how the NP distributions as obtained from MCTDHB oscillates between the characteristics of the Gross-Pitaevskii mean-field state and a (slightly) correlated one, which

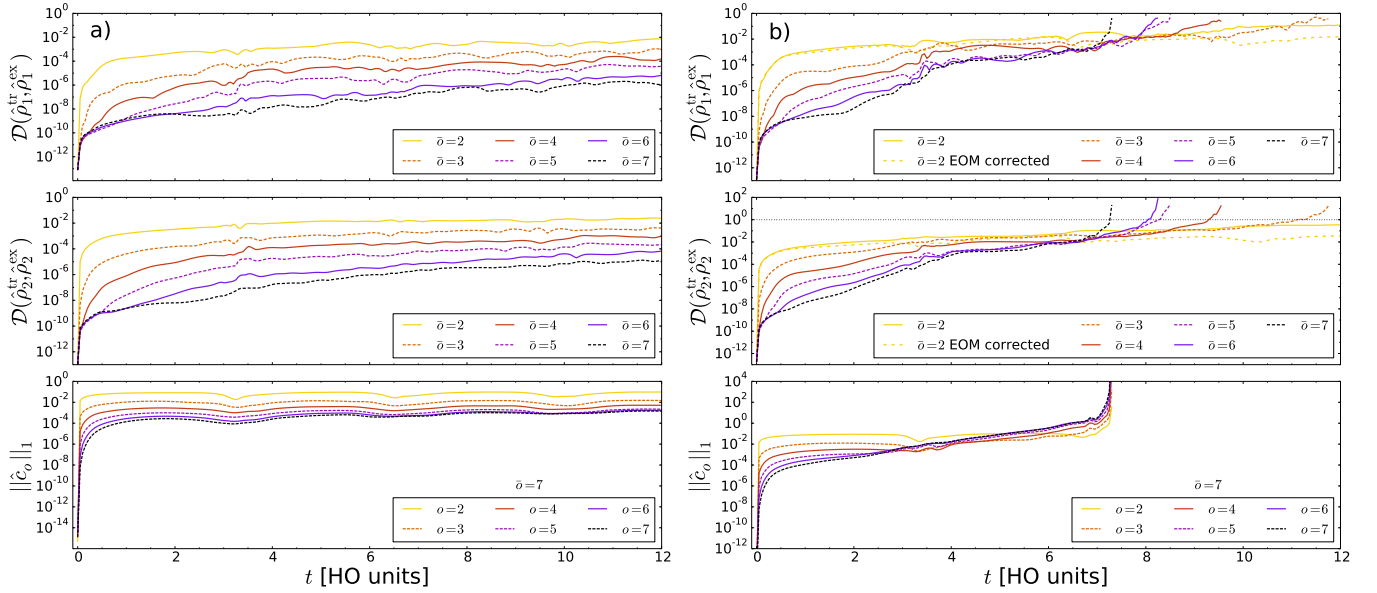


Figure 10. (color online) First and second row: Time evolution of the trace distance $\mathcal{D}(\hat{\rho}_o^{\text{tr}}, \hat{\rho}_o^{\text{ex}})$ between the MCTDHB and the truncated BBGKY prediction for the o -RDM ($o = 1, 2$) and various truncation orders \bar{o} . The dotted horizontal line at unity ordinate value indicate the upper bound for the trace distance between two density operators. Third row: Time-evolution of the cluster's trace-class norm $\|\hat{c}_o\|_1$ for $o = 1, \dots, 7$ obtained from the data of the $\bar{o} = 7$ simulations. Left column: $N = 10$ atoms. Right columns: $N = 30$. Otherwise, same parameters as in Figure 9.

is approximately synchronized to the strongest contraction and expansion of the density, respectively [see Figure 8 b)]. In contrast to the former case, however, we can converge the NPs to the MCTDHB results upon increasing the truncation order \bar{o} only for times $t \lesssim 5$ HO units. For all considered truncation orders, we witness an exponential-like instability in the 2-RDM NPs resulting in large negative eigenvalues while the 1-RDM stays positive semi-definite for the considered time-span. Fixing \bar{o} , we have observed also for this scenario that the lack of positive semi-definiteness of the o -RDMs happens in decreasing sequence with respect to the order o (not shown). Moreover, these instabilities in the 2-RDM NPs seem to be triggered by small positive NPs approaching zero from above, namely when the density approximately shrinks to its initial width, see e.g. Figure 11 (c.2). Finally, we have observed for the case $\bar{o} = 2$ that increasing the number of SPFs from $m = 4$ to $m = 8$ slightly enhances the time-scale on which the instability of the 2-RDM NPs takes place (not shown). This finding is reasonable since the projector $(\mathbb{1} - \hat{\mathbb{P}})$, occurring in the SPF EOM (5) of [1], projects onto a smaller subspace when increasing m such that the impact of the non-linearity in the SPF EOM is effectively reduced.

2. Reduced density operators

Comparing the BBGKY prediction for the complete 1- and 2-RDM with the corresponding MCTDHB results in terms of the trace-class distance in Figure 10 b), we see

that deviations emerge much faster as compared to the $N = 10$ case. At longer times, we also observe that the accuracy of the BBGKY results does not monotonously increase anymore with increasing \bar{o} . Moreover, the above mentioned instabilities also partly manifest themselves in $\mathcal{D}(\hat{\rho}_2^{\text{tr}}, \hat{\rho}_2^{\text{ex}})$ attaining unphysical values above unity. Finally, we also depict $\|\hat{c}_o\|_1$ as a measure for correlations in Figure 10 b). While the correlations are hierarchically ordered in decreasing sequence with respect to the order o up to $t \sim 2.7$ HO units, this ordering becomes reversed later on. This finding, however, is not conclusive, i.e. might be unphysical and related to the observed instability, since the values of $\|\hat{c}_o\|_1$ have been extracted from the BBGKY data with $\bar{o} = 7$ (in contrast to the tunneling scenario where the numerically exact \hat{c}_o have been used).

At this point, we shall remark that we expect a much better agreement for the $N = 30$ case when quenching to much lower interaction strengths $g \ll 0.2$ and thereby reducing the overall excitation energy.

3. Performance of the correction algorithms

Here, we again focus mainly on the performance of the correction algorithms applied to the $\bar{o} = 2$ BBGKY approach and comment later on larger truncation orders.

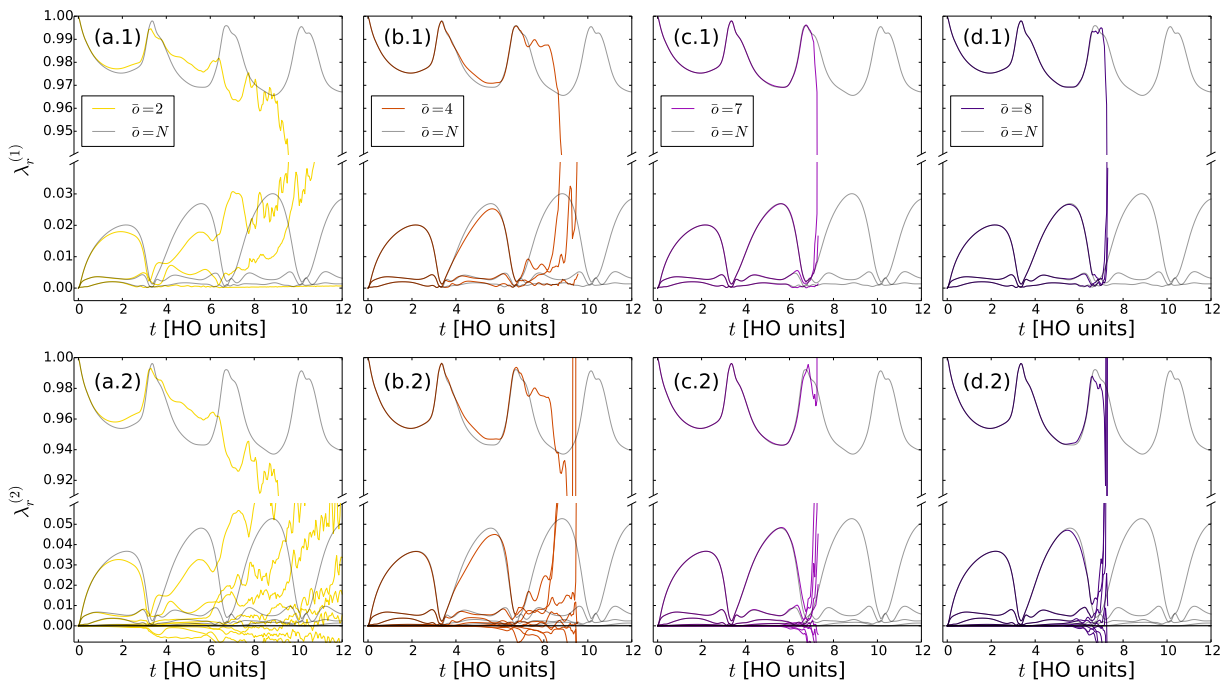


Figure 11. (color online) Top (bottom) row: Time-evolution of the 1-RDM (2-RDM) NPs for various truncation orders \bar{o} in comparison to the MCTDHB results. We note that the ordinates are broken into two parts for covering the whole range of relevant values. In some cases, this leads to discontinuous curves, see e.g. the $\bar{o} = 2$ curve in (a.2). Number of bosons: $N = 30$. Otherwise, same parameters as in Figure 9.

In Figure 12, we depict the spectrum³ of \hat{K}_2 as well as a close-up to the 2-RDM spectrum in the vicinity of zero for the uncorrected BBGKY approach, the minimal invasive RDM purification algorithm and the minimal invasive EOM correction algorithm. In the minimization problem underlying both correction algorithms, we have to find the optimal \hat{C}_2 which depends on $m^2(m+1)^2/4 = 100$ real-valued parameters. Being contraction-free and energy conserving leads to $m^2 + 1 = 17$ constraints. Moreover, \hat{C}_2 has to obey the parity symmetry of our problem imposing $m^4/8 + m^3/4 = 48$ further constraints (see Appendix H of [1]). Thereby, our system of linear constraints remains underdetermined as long as the number d of negative $\hat{\rho}_2$ eigenvalues and number d' of negative \hat{K}_2 eigenvalues obey $d + d' < 35$.

In Figure 12, we see that the minimal-invasive RDM purification algorithm clearly suppresses significant negative eigenvalues until $t \sim 2.5$ HO units. Thereafter, noticeably negative eigenvalue emerge but stay bounded from below until $t \sim 6$ HO units when a drastic instability kicks in. Thus, this iterative algorithm soon fails to converge after the maximal number of 500 iteration

steps. In order to understand the deeper reason of this failure, we have analyzed the spectrum of the updated operators $\hat{\rho}_2(t) + \alpha \hat{C}_2$ and $\hat{K}_2(t) + \alpha \hat{\Delta}_2$ for $\alpha \in [0, 1]$ and the first few iteration steps at such an instant in time (not shown). Thereby, we have found that while the tangent on a negative eigenvalue (with respect to α) indeed crosses zero as imposed by our constraints, level repulsion with other (in most cases negative) eigenvalues often hinders this negative eigenvalue to significantly move towards zero. We cannot rigorously prove that this is indeed the only mechanism for the breakdown of this iterative purification algorithm, of course.

Yet at least, this finding gives a useful hint why our non-perturbative, adaptive approach, the minimal invasive correction scheme of the 2-RDM EOM, gives very stable results [see Figure 12 (c.1) and (c.2)]. Actually, we observe that the D - and K -conditions are fulfilled to a good approximation much longer, namely for at least $t \leq 36$ HO unit (not shown). From Figure 12 (d), we furthermore infer that the integrator variably adapts its step-size, but in contrast to the Bose-Hubbard tunneling scenario no systematic enhancement of integrator steps is observed when $\hat{\rho}_2$ or \hat{K}_2 eigenvalues avoid each other in the vicinity of zero. Apparently, the though stabilized result features noticeable deviations from the MCTDHB results for the respective eigenvalues. Yet, we find that the overall accuracy of the $\bar{o} = 2$ results for the 1- and 2-RDM as measured by the trace-class distance is systematically improved for most times by correcting the

³ We note that the \hat{K}_2 spectra at $t = 0$ in the tunneling and the interaction-quench scenario differ although the system is initially a fully condensed BEC in both cases (see Figures 7 and 12). This is due to the fact that the \hat{K}_2 spectrum is sensitive to the total number of SPFs m even if not all of them are occupied.

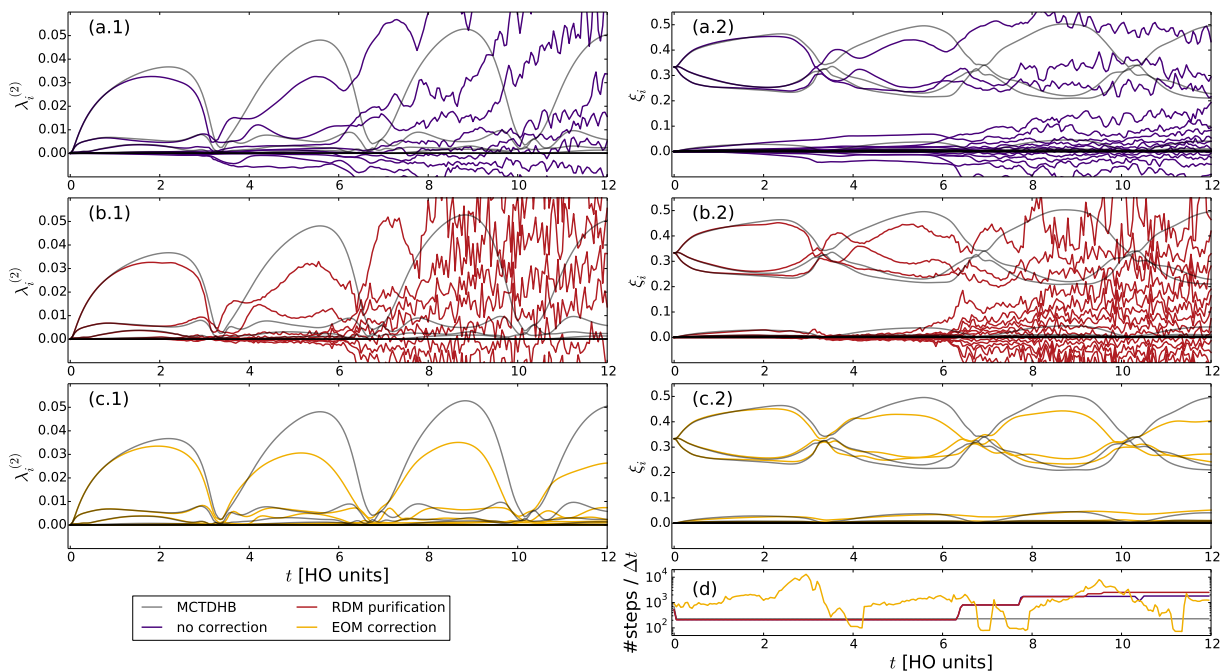


Figure 12. (color online) Comparison of the correction strategies outlined in Section V B of [1] (for the BBGKY hierarchy truncated at $\bar{o} = 2$), i.e. same as Figure 7 but for the interaction-quench scenario with $N = 30$ bosons. Parameters: threshold $\epsilon = -10^{-10}$, damping constant $\eta = 10$ HO units, write-out time-step $\Delta t = 0.05$ HO units, maximal number of iterations: 500. Otherwise, same parameters as in Figure 9.

2-RDM EOM, as one can infer from Figure 10 b).

In order to judge the accuracy of the EOM-corrected $\bar{o} = 2$ simulation more descriptively, we depict the deviations of its prediction for the reduced one-body density from the MCTDHB results in Figure 13. Note that this plot covers a longer time-span compared to the previous ones. As expected, we find that the deviations increase in time. Compared to the absolute values of the density, these deviations are, however, small and, most importantly, somewhat smaller than the deviations of corresponding Gross-Pitaevskii mean-field simulation from the $m = 4$ MCTDHB results (not shown). Finally, let us connect the errors in the one-body density to the errors measured by the trace-class distance $\mathcal{D}(\hat{\rho}_1^{\text{tr}}, \hat{\rho}_1^{\text{ex}})$ as depicted in Figure 10 b). For this purpose, we note that the density at position x can be expressed as the expectation value of the one-body observable $\hat{A}_1 = |x\rangle\langle x|$ featuring $\|\hat{A}_1\|_1 = 1$. Thereby, the inequality of Appendix B gives $|\rho_1^{\text{tr}}(x; t) - \rho_1^{\text{ex}}(x; t)| \leq 2\mathcal{D}(\hat{\rho}_1^{\text{tr}}(t), \hat{\rho}_1^{\text{ex}}(t))$, which is consistent with the results depicted in Figure 13.

Going to higher truncation orders by making the Mazziotti ansatz for the corresponding higher-order correction operators \hat{C}_o unfortunately does not improve the BBGKY results, as already observed in the tunneling scenario. While the iterative RDM purification scheme fails to prevent the instabilities, we observe the same obstacle for the EOM correction algorithm as previously encountered, namely the optimization problem at order $o = 2$ lacking a solution (results not shown). Yet due to the

very promising results of the EOM correction algorithm when truncating the BBGKY hierarchy at order $\bar{o} = 2$, we believe that extending the EOM correction algorithm to higher orders without employing the Mazziotti ansatz for the correction operator is a highly promising direction to go.

IV. CONCLUSIONS

While we have provided the theoretical framework of the truncated BBGKY hierarchy for simulating the quantum dynamics of few-particle reduced density operators of an ultracold bosonic many-body system in the immediately preceding work [1], we have provided here extensive applications. The central aim of this work is to systematically study the impact of the BBGKY hierarchy truncation order \bar{o} on the numerically obtained results where the highly efficient formulation of the theory in [1] allows us for going to truncation orders as high as $\bar{o} = 12$. For this purpose, we have considered both a tunneling scenario where a Bose-Einstein condensate fragments into a two-fold fragmented, highly entangled state and thus strong correlations emerge, and an interaction-quench scenario where a Bose-Einstein condensate becomes weakly depleted when performing collective oscillations. While the former scenario is based on the Bose-Hubbard dimer model where we may use time-independent Wannier states for representing the reduced density operators

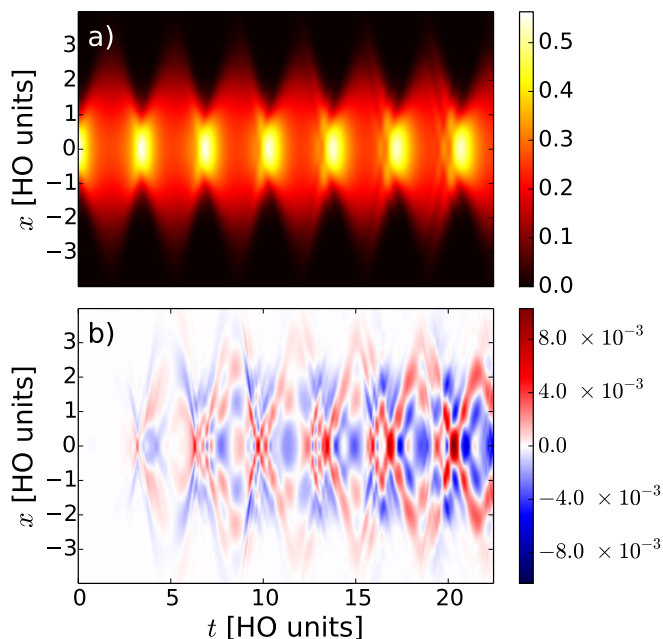


Figure 13. (color online) Subfigure a): Time-evolution of the reduced one-body density $\rho_1^{\text{ex}}(x; t)$ as obtained from MCTDHB on a longer time-scale. Subfigure b): Absolute deviation $\rho_1^{\text{tr}}(x; t) - \rho_1^{\text{ex}}(x; t)$ of the reduced one-body density $\rho_1^{\text{tr}}(x; t)$ as obtained from the BBGKY approach truncated at $\bar{o} = 2$ and stabilized by the minimal-invasive EOM correction algorithm with $\epsilon = -10^{-10}$ and $\eta = 10$ HO units. Number of bosons: $N = 30$. Otherwise, same parameters as in Figure 9.

(RDMs), we solve in the second scenario the truncated BBGKY hierarchy as derived from the variational Multi-Configuration Time-Dependent Hartree method for Bosons (MCTDHB) [1, 7] and thereby employ dynamically optimized single-particle functions for efficiently representing the RDMs. The truncated BBGKY results are comprehensively evaluated by inspecting a variety of observables, covering descriptive ones such as the atomic density but also the eigenvalues of the low-order RDMs and their trace-class distances to the corresponding numerically exact and MCTDHB results in the first and second scenario, respectively.

In all applications, we have found that the short-time dynamics can be highly accurately described by the truncated BBGKY approach, where the accuracy of the results systematically improves with increasing truncation order \bar{o} . At longer times, the BBGKY gives also excellent results with controllable accuracy for the interaction-quench scenario and not too high excitation energies. For higher excitation energies as well as in the tunneling scenario, however, we obtain only faithful results up to a certain time even if we truncate the hierarchy at the highest non-trivial order $\bar{o} = N - 1$ with N denoting the total number of particles. After that time, the accuracy does not monotonously improve with increasing truncation order and instabilities emerge, manifesting themselves in an exponential-like decrease of RDM eigenvalues to negative

values. By inspecting the exact numerical results for the tunneling scenario, we find that few-particle correlations on all orders quickly play a significant role and eventually N -particle correlations dominate because the total system evolves into a NOON-state. This finding indicates that the long-time physics of this scenario prevents to use a truncation approximation which is based on neglecting $(\bar{o} + 1)$ -particle correlations.

Nevertheless, it is important to clearly separate the stability properties of the truncated BBGKY equations of motion (EOM) from accuracy issues because (i) it is not desirable to have a highly accurate theory which is exponentially unstable under slight e.g. numerical perturbations and (ii) also a not highly accurate truncation approximation may give useful, sufficiently accurate results for low-dimensional observables such as the density if the EOM are sufficiently stable. In order to disentangle stability issues from the accuracy of the results, we have performed an in-depth analysis of the observed exponential-like instabilities. In all examples, we witness that the instability sets in at the truncation order \bar{o} and then propagates down to lower orders meaning that o -particle RDMs lack to be positive semi-definite in decreasing sequence with respect to the order o . The time until which the highest-order RDM, $\hat{\rho}_{\bar{o}}$, stays positive semi-definite only gradually increases with the truncation order \bar{o} . Upon increasing \bar{o} , the most important RDMs for calculating relevant observables for ultracold systems, $\hat{\rho}_1$ and $\hat{\rho}_2$, are found to stay a bit longer positive semi-definite in some examples, in others, however, the opposite holds. That the instabilities set in more rapidly with increasing truncation order \bar{o} might be explained by the fact that the cluster-expansion based truncation approximation (see Section I B 3 of [1]) constitutes a polynomial of degree $(\bar{o} + 1)$ in $\hat{\rho}_1$ and of degree $\lfloor (\bar{o} + 1)/o \rfloor$ in the cluster \hat{c}_o . Thereby, the non-linearity of the EOM is effectively enhanced for increasing \bar{o} . Moreover, the instabilities often take place when the lowest RDM eigenvalues undergo an avoided crossing in the vicinity of zero.

Ultimately, these instabilities emerge due to the applied truncation approximation, which conserves the RDM compatibility and energy as well as respects symmetries such as the parity invariance if existent, but does not ensure that important necessary representability conditions such as the positive semi-definiteness of $\hat{\rho}_o$ and of the one-particle-one-hole RDM are fulfilled [1]. In order to enforce such representability conditions and stabilize the EOM for a given truncation order \bar{o} (independently of the accuracy of the results), we have evaluated the two novel correction algorithms developed in [1]. Both strategies aim at ensuring the positive semi-definiteness of $\hat{\rho}_2$ and the (modified) one-particle-one-whole RDM as defined in [43] in a minimal-invasive and energy-conserving way by solving an optimization problem. For higher orders, the Mazziotti ansatz [44] for the correction operator is chosen. The first strategy corrects the solution of the truncated BBGKY EOM after each small time-step Δt by iteratively adding a correction operator which

raises negative eigenvalues to zero in first order perturbation theory. Unfortunately, this iterative algorithm does not lead to a significant stabilization over a reasonable time-span and soon fails to converge most likely due to level-repulsion of the lowest eigenvalues which cannot be overcome by a perturbative approach. Yet the second approach, which corrects the truncated BBGKY EOM themselves in a minimal-invasive, energy-conserving way such that negative eigenvalues are exponentially damped to zero, has proven to stabilize the dynamics for long times if applied to the truncation order $\bar{o} = 2$. This highlights that a successful stabilization of the dynamics requires a non-perturbative control of the low-lying spectrum of e.g. $\hat{\rho}_2$. Moreover, the long-time results of the EOM-corrected BBGKY approach for various observables are also qualitatively correct in the case of the interaction-quench scenario. Yet extending the EOM-correction algorithm to higher orders by the Mazziotti ansatz has been found to lead to stiff EOM or the optimization problem at order $o = 2$ lacking a solution.

Due to the success for $\bar{o} = 2$, however, we believe that research on how to properly and efficiently extend the EOM-correction algorithm to higher orders constitutes a highly promising route for the future, which can result in a robust BBGKY approach with controllable accuracy for broad applications. A second future line of research should address how to improve the truncation approximation of the BBGKY hierarchy for bosonic systems with a definite number of particles, where the existing literature is rather sparse compared to the fermionic case. We note here that all results of this work rely on the chosen definition of few-particle correlations, of course. One novel approach for the truncation might involve to use machine-learning techniques such as artificial neural networks for deducing the unknown collision integral at the truncation order in combination with an EOM correction algorithm for stabilizing the dynamics. In any case, the theoretical framework and the highly efficient formulation of the theory as provided in [1] together with the deep empirical insights of this work serve as an important step in the direction of establishing the BBGKY approach as a simulation tool for ultracold atomic systems.

ACKNOWLEDGMENTS

The authors thank Iva Březinová, Joachim Burgdörfer, David A. Mazziotti, Hans-Dieter Meyer, Angel Rubio, Johannes M. Schurer and Jan Stockhofe for fruitful discussions. This work has been supported by the excellence cluster “The Hamburg Centre for Ultrafast Imaging - Structure, Dynamics and Control of Matter at the Atomic Scale” of the Deutsche Forschungsgemeinschaft.

Appendix A: Integration of the truncated BBGKY EOM

In both scenarios, we employ the variable-coefficient ordinary differential equation solver ZVODE [42] for integrating the EOM (5),(6) of [1]. The conservation of hermiticity of the RDMs is numerically ensured by only propagating the lower triangle of the matrix-valued EOM (6) of [1], which at the same time reduces the number of variables to be integrated. Since the applied truncation approximation conserves the compatibility of the RDMs, we propagate only the BBGKY EOM (6) of [1] at the truncation order \bar{o} and obtain the RDMs of lower order by partial tracing.

Appendix B: Trace distance and expectation value of observables

Here, we briefly review why the trace distance $\mathcal{D}(\hat{\rho}_o^{\text{tr}}, \hat{\rho}_o^{\text{ex}})$ constitute a bound for the difference in the prediction for the expectation value of any given trace-class o -body observable \hat{A}_o . Introducing the spectral decompositions $\hat{A}_o = \sum_r \alpha_r |a_r\rangle\langle a_r|$ and $\hat{\rho}_o^{\text{tr}} - \hat{\rho}_o^{\text{ex}} = \sum_r \beta_r |b_r\rangle\langle b_r|$, we may estimate

$$\begin{aligned} |\text{tr}(\hat{A}_o \hat{\rho}_o^{\text{tr}}) - \text{tr}(\hat{A}_o \hat{\rho}_o^{\text{ex}})| &\leq \sum_r |\beta_r| |\langle b_r | \hat{A}_o | b_r \rangle| \quad (\text{B1}) \\ &\leq \sum_{r,s} |\alpha_s| |\beta_r| |\langle b_r | a_s \rangle|^2 \leq \sum_{r,s} |\alpha_s| |\beta_r| \\ &= 2 \|\hat{A}_o\|_1 \mathcal{D}(\hat{\rho}_o^{\text{tr}}, \hat{\rho}_o^{\text{ex}}). \end{aligned}$$

-
- [1] S. Krönke and P. Schmelcher. The BBGKY hierarchy for ultracold bosonic systems: I. Theoretical framework. *To be published*.
- [2] C. J. Pethick and H. Smith. *Bose-Einstein Condensates in Dilute Gases*. Cambridge University Press, 2nd edition, 2008.
- [3] I. Bloch, J. Dalibard, and W. Zwerger. Many-body physics with ultracold gases. *Rev. Mod. Phys.*, 80:885, 2008.
- [4] M. Lewenstein, A. Sanpera, and V. Ahufinger. *Ultracold Atoms in Optical Lattices: Simulating quantum many-body systems*. Oxford University Press, 2012.
- [5] U. Schollwöck. The density-matrix renormalization group in the age of matrix product states. *Ann. Phys. (NY)*, 326:96, 2011.
- [6] M. L. Wall and L. D. Carr. Out-of-equilibrium dynamics with matrix product states. *New J. Phys.*, 14:125015, 2012.
- [7] O. E. Alon, A. I. Streltsov, and L. S. Cederbaum. Multiconfigurational time-dependent Hartree method for bosons: Many-body dynamics of bosonic systems. *Phys. Rev. A*, 77:033613, 2008.
- [8] N. N. Bogoliubov. *The Dynamical Theory in Statistical Physics*. Hindustan Pub. Corp., Delhi, 1965.

- [9] M. Born and H. S. Green. A general kinetic theory of liquids. iv. quantum mechanics of fluids. *Proc. R. Soc. London, Ser. A*, 191:168, 1947.
- [10] J. Kirkwood. The Statistical Mechanical Theory of Transport Processes I. General Theory. *J. Chem. Phys.*, 14:180, 1946.
- [11] J. Yvon. Une méthode d'étude des corrélations dans les fluides quantiques en équilibre. *Nucl. Phys.*, 4:1, 1957.
- [12] M. Bonitz. *Quantum Kinetic Theory*, volume 33 of *Teubner-Texte zur Physik*. B. G. Teubner, 1998.
- [13] A. Akbari, M. J. Hashemi, A. Rubio, R. M. Nieminen, and R. van Leeuwen. Challenges in truncating the hierarchy of time-dependent reduced density matrices equations. *Phys. Rev. B*, 85:235121, 2012.
- [14] D. B. Jeffcoat and E. A. DePrince. N-representability-driven reconstruction of the two-electron reduced-density matrix for a real-time time-dependent electronic structure method. *J. Chem. Phys.*, 141:214104, 2014.
- [15] M. Tohyama and P. Schuck. Truncation scheme of time-dependent density-matrix approach. *Eur. Phys. J. A*, 50:77, 2014.
- [16] M. Tohyama and P. Schuck. Truncation scheme of time-dependent density-matrix approach ii. *Eur. Phys. J. A*, 53:186, 2017.
- [17] F. Lackner, I. Březinová, T. Sato, K. L. Ishikawa, and J. Burgdörfer. Propagating two-particle reduced density matrices without wave functions. *Phys. Rev. A*, 91:023412, 2015.
- [18] F. Lackner, I. Březinová, T. Sato, K. L. Ishikawa, and J. Burgdörfer. High-harmonic spectra from time-dependent two-particle reduced-density-matrix theory. *Phys. Rev. A*, 95:033414, 2017.
- [19] P. Elliott and N. T. Maitra. Density-matrix propagation driven by semiclassical correlation. *Int. J. Quant. Chem.*, 116:772, 2016.
- [20] M. Kira. Excitation picture of an interacting Bose gas. *Ann. Phys. (N. Y.)*, 351:200, 2014.
- [21] M. Kira. Coherent quantum depletion of an interacting atom condensate. *Nat. Commun.*, 6, 2015.
- [22] M. Kira. Hyperbolic Bloch equations: atom-cluster kinetics of an interacting Bose gas. *Ann. Phys. (N. Y.)*, 356:185, 2015.
- [23] T. Köhler and K. Burnett. Microscopic quantum dynamics approach to the dilute condensed Bose gas. *Phys. Rev. A*, 65:033601, 2002.
- [24] T. Köhler, T. Gasenzer, and K. Burnett. Microscopic theory of atom-molecule oscillations in a Bose-Einstein condensate. *Phys. Rev. A*, 67:013601, 2003.
- [25] A. Vardi and J. R. Anglin. Bose-Einstein Condensates beyond Mean Field Theory: Quantum Backreaction as Decoherence. *Phys. Rev. Lett.*, 86:568, 2001.
- [26] J. R. Anglin and A. Vardi. Dynamics of a two-mode Bose-Einstein condensate beyond mean-field theory. *Phys. Rev. A*, 64:013605, 2001.
- [27] I. Tikhonenkov, J. R. Anglin, and A. Vardi. Quantum dynamics of Bose-Hubbard Hamiltonians beyond the Hartree-Fock-Bogoliubov approximation: The Bogoliubov back-reaction approximation. *Phys. Rev. A*, 75:013613, 2007.
- [28] F. Trimborn, D. Witthaut, H. Hennig, G. Kordas, T. Geisel, and S. Wimberger. Decay of a Bose-Einstein condensate in a dissipative lattice - the mean-field approximation and beyond. *Eur. Phys. J. D*, 63:63, 2011.
- [29] D. Witthaut, F. Trimborn, H. Hennig, G. Kordas, T. Geisel, and S. Wimberger. Beyond mean-field dynamics in open Bose-Hubbard chains. *Phys. Rev. A*, 83:063608, 2011.
- [30] G. Kordas, D. Witthaut, P. Buonsante, A. Vezzani, R. Burioni, A. I. Karanikas, and S. Wimberger. The Dissipative Bose-Hubbard Model. Methods and Examples. *Eur. Phys. J.*, 224:2127, 2015.
- [31] S. Raghavan, A. Smerzi, S. Fantoni, and S. R. Shenoy. Coherent oscillations between two weakly coupled Bose-Einstein condensates: Josephson effects, π oscillations, and macroscopic quantum self-trapping. *Phys. Rev. A*, 59:620, 1999.
- [32] A. Smerzi, S. Fantoni, S. Giovanazzi, and S. R. Shenoy. Quantum Coherent Atomic Tunneling between Two Trapped Bose-Einstein Condensates. *Phys. Rev. Lett.*, 79:4950, 1997.
- [33] G. J. Milburn, J. Corney, E. M. Wright, and D. F. Walls. Quantum dynamics of an atomic Bose-Einstein condensate in a double-well potential. *Phys. Rev. A*, 55:4318, 1997.
- [34] K. Sakmann, A. I. Streltsov, O. E. Alon, and L. S. Cederbaum. Exact Quantum Dynamics of a Bosonic Josephson Junction. *Phys. Rev. Lett.*, 103:220601, 2009.
- [35] K. Sakmann, A. I. Streltsov, O. E. Alon, and L. S. Cederbaum. Quantum dynamics of attractive versus repulsive bosonic Josephson junctions: Bose-Hubbard and full-Hamiltonian results. *Phys. Rev. A*, 82:013620, 2010.
- [36] K. Sakmann, A. I. Streltsov, O. E. Alon, and L. S. Cederbaum. Universality of fragmentation in the schrödinger dynamics of bosonic josephson junctions. *Phys. Rev. A*, 89:023602, 2014.
- [37] B. Gertjerenken and C. Weiss. Beyond-mean-field behavior of large Bose-Einstein condensates in double-well potentials. *Phys. Rev. A*, 88:033608, 2013.
- [38] M. Albiez, R. Gati, J. Fölling, S. Hunsmann, M. Cristiani, and M. K. Oberthaler. Direct Observation of Tunneling and Nonlinear Self-Trapping in a Single Bosonic Josephson Junction. *Phys. Rev. Lett.*, 95:010402, 2005.
- [39] P.-O. Löwdin. Quantum Theory of Many-Particle Systems. I. Physical Interpretations by Means of Density Matrices, Natural Spin-Orbitals, and Convergence Problems in the Method of Configurational Interaction. *Phys. Rev.*, 97:1474, 1955.
- [40] K. Sakmann, A. I. Streltsov, O. E. Alon, and L. S. Cederbaum. Reduced density matrices and coherence of trapped interacting bosons. *Phys. Rev. A*, 78:023615, 2008.
- [41] M. A. Nielsen and I. L. Chuang. *Quantum Computation and Quantum Information*. Cambridge University Press, 2000.
- [42] A. C. Hindmarsh. *ODEPACK, a Systematized Collection of ODE Solvers*, page 55. Scientific Computing. North-Holland, Amsterdam, 1983.
- [43] C. Garrod and J. K. Percus. Reduction of the N-Particle Variational Problem. *J. Math. Phys.*, 5:1756, 1964.
- [44] D. A. Mazziotti. Purification of correlated reduced density matrices. *Phys. Rev. E*, 65:026704, 2002.
- [45] C. Menotti and S. Stringari. Collective oscillations of a one-dimensional trapped bose-einstein gas. *Phys. Rev. A*, 66:043610, 2002.
- [46] H. Moritz, T. Stöferle, M. Köhl, and T. Esslinger. Exciting collective oscillations in a trapped 1d gas. *Phys. Rev. Lett.*, 91:250402, 2003.

- [47] S. Bauch, K. Balzer, C. Henning, and M. Bonitz. Quantum breathing mode of trapped bosons and fermions at arbitrary coupling. *Phys. Rev. B*, 80:054515, 2009.
- [48] J. W. Abraham and M. Bonitz. Quantum breathing mode of trapped particles: From nanoplasmas to ultracold gases. *Contrib. Plasma Phys.*, 54:27, 2014.
- [49] R. Schmitz, S. Krönke, L. Cao, and P. Schmelcher. Quantum breathing dynamics of ultracold bosons in one-dimensional harmonic traps: Unraveling the pathway from few-to many-body systems. *Phys. Rev. A*, 88:043601, 2013.
- [50] W. Tschischik, R. Moessner, and M. Haque. Breathing mode in the bose-hubbard chain with a harmonic trapping potential. *Phys. Rev. A*, 88:063636, 2013.
- [51] B. Fang, G. Carleo, A. Johnson, and I. Bouchoule. Quench-induced breathing mode of one-dimensional bose gases. *Phys. Rev. Lett.*, 113:035301, 2014.
- [52] M. Pyzh, S. Krönke, C. Weitenberg, and P. Schmelcher. Spectral properties and breathing dynamics of a few-body Bose-Bose mixture in a 1d harmonic trap. *arXiv:1707.03758 [cond-mat, physics:quant-ph]*, 2017.
- [53] E. Haller, M. Gustavsson, M. J. Mark, J. G. Danzl, R. Hart, G. Pupillo, and Hanns-Christoph H.-C. Nägerl. Realization of an excited, strongly correlated quantum gas phase. *Science*, 325:1224, 2009.
- [54] J.C. Light and T. Carrington. Discrete-variable representations and their utilization. *Adv. Chem. Phys.*, 114:263, 2000.
- [55] M. H. Beck, A. Jäckle, G. A. Worth, and H. D. Meyer. The multiconfiguration time-dependent hartree (mctdh) method: a highly efficient algorithm for propagating wavepackets. *Physics Reports*, 324:1, 2000.